# Spatiotemporal dynamics near the onset of convection for binary mixtures in cylindrical containers

Isabel Mercader,* Arantxa Alonso, and Oriol Batiste
*Departament de Física Aplicada, Universitat Politècnica de Catalunya, Mòdul B4, 08034 Barcelona, Spain*
(Received 8 August 2007; published 20 March 2008)

Pattern selection near the onset of convection in a cylindrical container heated from below is investigated numerically for a water-ethanol mixture, with parameter values and boundary conditions relevant to experiments. The Boussinesq three-dimensional equations for binary fluid convection are simulated for cylinders of aspect ratio $\Gamma=11$ and 10.5 ($\Gamma\equiv R/d$, where $R$ is the radius of the cell and $d$ its height). The onset of convection occurs via a subcritical Hopf bifurcation in which the critical mode is strongly influenced by small variations of the aspect ratio of the cell. During the linear regime, an $m=1$ azimuthal mode consisting of radially traveling waves grows in amplitude in the $\Gamma=11$ cell, while an $m=0$ azimuthal mode is selected in the $\Gamma=10.5$ cylinder. As convection evolves, simulations for subcritical and supercritical Rayleigh numbers reveal differences in the dynamics. Very close to the critical value, convection is erratic and focuses along one or more diameters of the cell; growths and collapses of the convection amplitude take place, but convection eventually dies away for subcritical values and persists for slightly supercritical values. For larger supercritical values, convection grows progressively in amplitude, and patterns consist of traveling-wave regions of convection initially focused near the cell center, though expanding slowly until a large-amplitude state is reached. Depending on the reduced Rayleigh number, the final state can be a nonsteady state filling the cell or a disordered confined state.

DOI: 10.1103/PhysRevE.77.036313 PACS number(s): 47.20.Bp, 47.54.−r, 47.55.pd, 47.27.ek

## I. INTRODUCTION

Convection in vertically heated binary-liquid mixtures is an excellent system for the study of pattern formation, especially for negative separation ratio mixtures, $S<0$. In such mixtures, the primary bifurcation is subcritical and gives rise to a state of oscillatory convection. In large annular and rectangular containers, the linearly unstable state at the onset usually evolves either to a traveling-wave state or to stationary rolls that are called states of stationary overturning convection. Nevertheless, experiments on these geometries, usually performed on water-ethanol mixtures, show that a great variety of states can arise near the onset of convection, including states of localized traveling-wave convection (pulses of traveling waves coexist with regions of quiescent fluid), states characterized by repeated bursts of amplitude, or regimes exhibiting spatiotemporal chaos [1–5]. If the container is sufficiently narrow, the resulting system is approximately two dimensional and can be modeled neglecting the effect of the cell thickness. The numerical work dealing with the study of several aspects of the dynamics in two-dimensional containers is abundant (e.g., [6–15]).

With the aim of investigating if the same types of states are found in truly three-dimensional geometries, several experiments on cylindrical cells have been done [16–19]. The results of these experimental works indicate that new behavior prevails. Waves that travel in the radial direction are present, and traveling-wave convection patterns typically consist of several competing domains of traveling waves propagating in different directions. Transient localized pulses of traveling-wave convection similar to the states found in annular cells were observed, but these pulses either decayed back to pure conduction or grew to fill the cell.

In the experimental observations of Lerman *et al.* [16–18], $S\approx-0.08$ water-ethanol mixtures are used in cylindrical containers of aspect ratio $\Gamma\approx 11$ ($\Gamma=10.91, 11.53$). Convection immediately above the onset consists of a superposition of radially inward and outward traveling waves filling the cell. The wave amplitude presents a sinusoidal azimuthal modulation, which is very sensitive to the actual value of the aspect ratio. While for the $\Gamma=10.91$ cell the dominant azimuthal modes are odd, a small variation of 0.5 in the value of $\Gamma$ causes the even modes to be favored at the onset. As the amplitude of convection grows, higher azimuthal modes become important and convection gets localized along one or more diameters of the cell. The focused lines of convection then collapse and can result in radially localized pulses, very similar to the ones observed in long annular cells, or in localized but disordered regions of convection. However, the localized states are not stable and always lead to a state in which the entire container is filled with convection rolls or they decay back to the conduction state and the process begins again. Apart from these confined states, on one occasion a wall state consisting of a narrow ring of azimuthal traveling waves very close to the wall and pure conduction in the interior was observed [17].

The other available experimental study on water-ethanol mixtures in cylindrical containers is the work of La Porta and Surko [19]. They consider a mixture with a much stronger Soret coupling $S=-0.24$, and survey the patterns arising in a $\Gamma=26$ aspect ratio cell. The larger aspect ratio cell decreases the influence of the boundaries on the dynamics. Disordered states consisting of many small domains of traveling waves are observed in which a significant part of the pattern does not interact with the boundaries. Over time, these domains

*isabel@fa.upc.edu

 

increase their size and the boundaries become important again. The resulting patterns typically consist of three or four domains of traveling waves whose dynamics seems to be controlled by the domain boundaries. The character of the patterns changes as the value of the control parameter increases, and rotating patterns are observed. Above a certain value, stationary overturning convection consisting of regions of straight rolls is observed.

The numerical work on this system is scarce [20], since these types of three-dimensional computations are very costly. One of the few previous numerical works on this system deals with the stability analysis of the conduction state in cylindrical containers of aspect ratios 2.76 and 11 [21]. In this work, Mercader *et al.* show that the eigenfunctions take the form of different types of right-handed or left-handed rigidly rotating spirals, or of convection rolls which travel radially inward and outward. Additionally, as in pure fluid convection in a rotating cylinder, the modes can be either spatially extended body modes or wall modes confined to the outer wall of the cylinder. In a more recent work, Millour *et al.* [22] study binary fluid convection in a vertical cylinder of aspect ratio 0.5 for two types of lateral boundary conditions using time integration of the axisymmetric equations.

The high performance achieved by present computers makes it possible nowadays to address fully three-dimensional (3D) computations. However, as far as the authors know, the major part of the recent numerical work dealing with fully 3D simulations of convection in cylindrical geometry is aimed at studying pure fluid convection. Convective patterns including multiroll patterns, targets, and spirals were obtained in moderate aspect ratio cells by Rüdiger and Feudel [23] ($\Gamma=4$) and by Leong [24] ($\Gamma=2,4$). Recently, time-dependent states arising in $1.45\leq\Gamma\leq1.57$ cells have been analyzed in the work of Borońska and Tuckerman [25]. On the other hand, the effects of rotation in pure fluid convection in cylinders have also been studied [26–30].

The present work is concerned with the direct numerical simulation of binary fluid convection in shallow vertical three-dimensional cells. We have developed an efficient three-dimensional time-evolution spectral code that solves the full convection equations in cylindrical coordinates. We describe and discuss the spatiotemporal dynamics arising near the onset of convection in $\Gamma=11$ and 10.5 cylindrical cells, extending the preliminary results presented in [31]. The parameters we consider are those used in one of the stability analyses included in [21], which are very similar to the experimental values used in [16–18].

With our work we wish to contribute to the understanding of the dynamics in three-dimensional convective layers of binary mixtures, since many features remain unclear. Confined convection similar to that observed in two-dimensional systems has been obtained experimentally, but, unlike in those systems, the pulses of convection do not seem to persist indefinitely in cylindrical cells. A more detailed exploration, varying the value of the separation ratio, which is known to influence the dynamics strongly, is needed to confirm whether stable confined convection is possible or not, and to provide an explanation. Another fundamental question is to what extent the arising dynamics is influenced by the lateral boundaries (shape and size) or whether it is determined mainly by the intrinsic features of the system. This problem is addressed in a very recent experimental work [32], where the global dynamics of traveling-wave patterns in circular, rectangular, and stadium-shaped cells is analyzed.

The paper is organized as follows. In the next section we write the equations governing the behavior of the system and describe the numerical tools we have used to solve them. In the following section, we discuss the features of the dynamics in the neighborhood of the onset of convection: the linear transient in $\Gamma=11$ and 10.5 cylinders, the nonlinear evolution for slightly subcritical and supercritical Rayleigh numbers in a $\Gamma=11$ cylinder, and, finally, the nonlinear evolution in a $\Gamma=10.5$ cell. To conclude, the main results and achievements of the work are summarized.

## II. EQUATIONS AND NUMERICAL TOOLS

We consider Boussinesq binary fluid convection in a cylinder of height $d$ and radius $R$. The radial aspect ratio of the cylinder is defined as $\Gamma=R/d$. The cylinder is heated from below, $\Delta T$ being the temperature difference between the lids, and the mixture is in the presence of vertical gravity $\mathbf{g}=-g\hat{\mathbf{e}}_z$. Scaling length with the height of the layer $d$, time with the vertical thermal diffusion time $d^2/\kappa$, $\kappa$ being the thermal diffusivity, and temperature with $\Delta T$, the nondimensional equations that describe the dynamics are

$$\boldsymbol{\nabla}\cdot\mathbf{u}=0, \tag{1}$$

$$\partial_t\mathbf{u}+(\mathbf{u}\cdot\boldsymbol{\nabla})\mathbf{u}=-\boldsymbol{\nabla}p+\sigma\boldsymbol{\nabla}^2\mathbf{u}+R\sigma[(1+S)\Theta+S\eta]\hat{\mathbf{e}}_z, \tag{2}$$

$$\partial_t\Theta+(\mathbf{u}\cdot\boldsymbol{\nabla})\Theta=w+\boldsymbol{\nabla}^2\Theta, \tag{3}$$

$$\partial_t\eta+(\mathbf{u}\cdot\boldsymbol{\nabla})\eta=-\boldsymbol{\nabla}^2\Theta+\tau\boldsymbol{\nabla}^2\eta. \tag{4}$$

Here, $\mathbf{u}=(u,v,w)$ is the velocity field in cylindrical coordinates $(r,\phi,z)$, $\Theta$ denotes the departure of temperature from the conduction profile, $\Theta=(T-T_c)/\Delta T$, and $\eta=-(C-C_c)/(C_0(1-C_0)S_T\Delta T)-\Theta$, where $T$ and $C$ are the fields of temperature and concentration of the denser component, $T_0$ and $C_0$ are their mean values, and $S_T$ is the Soret coefficient. Binary fluid convection is described by four dimensionless numbers, the Rayleigh number $R$, the Prandtl number $\sigma$, the Lewis number $\tau$, and the separation ratio $S$, defined as

$$R=\frac{\alpha\Delta T g d^3}{\kappa\nu},\quad \sigma=\frac{\nu}{\kappa},\quad \tau=\frac{D}{\kappa},\quad S=C_0(1-C_0)\frac{\beta}{\alpha}S_T,$$

where $\alpha$ and $\beta$ are the thermal and concentration expansion coefficients, $\kappa$ and $D$ are the thermal and mass diffusivities, and $\nu$ is the kinematic viscosity. The Rayleigh number is the control parameter of the system and measures the strength of the imposed temperature gradient. The Prandtl number relates momentum diffusion to heat diffusion, while the Lewis number relates concentration diffusion to heat diffusion. The separation ratio gives the coupling between the thermal and concentration density gradients. A negative value of $S$ indi-

cates that the concentration density gradient opposes the thermal density gradient, and tends to stabilize the fluid layer against thermal convection. For small $\tau$ and sufficiently negative values of $S$, the onset of convection is a Hopf bifurcation to a state of oscillatory convection.

For the boundary conditions, we consider a no-slip, no-flux, fixed temperature boundary at the top and bottom plates, and a no-slip, no-flux, insulating boundary on the lateral wall,

$$\mathbf{u} = \Theta = \partial_z \eta = 0 \quad \text{on} \quad z = 0,1, \tag{5}$$

$$\mathbf{u} = \partial_r \Theta = \partial_r \eta = 0 \quad \text{on} \quad r = \Gamma. \tag{6}$$

As a measure of the heat transport by convection, we use the Nusselt number Nu, defined as the ratio of heat flux through the top plate to that of the corresponding conductive solution:

$$\mathrm{Nu} = 1 - A^{-1} \int_A \partial_z \Theta|_{z=1} dA,$$

where $A$ is the area of the cylinder lids.

To estimate the contribution to the solution of each azimuthal Fourier mode $m$, we will also evaluate the kinetic energy contained on them defined by

$$E_k^m = \frac{4}{\Gamma^2} \int_{z=0}^{z=1} \int_{r=0}^{r=\Gamma} \mathbf{u}_m \cdot \mathbf{u}_m r \, dr \, dz.$$

To integrate the equations in time, we have used the second-order time-splitting method proposed in [33] combined with a pseudospectral method for the spatial discretization, Galerkin-Fourier in the azimuthal coordinate $\phi$, and Chebyshev collocation in $r$ and $z$. The radial dependence of the functions is approximated by a Chebyshev expansion between $-R$ and $R$, but forcing the proper parity of the variables at the origin [34]. For instance, the scalar field $\Theta$ has an even parity $\Theta(-r,\phi)=\Theta(r,\phi+\pi)$, the vertical velocity $w$ and $\eta$ obey the same even parity condition, whereas $u$ and $v$ are odd functions. To avoid including the origin in the mesh grid, we have used an odd number of Gauss-Lobatto points in $r$, and we have enforced the equations only in the interval $(0,R]$. We have used the standard combination $u_+=u+iv$ and $u_-=u-iv$ in order to obtain, as a result of the splitting, Helmholtz equations for all the variables $\Theta$, $\eta$, $w$, $u_+$, and $u_-$. For each Fourier mode, these equations have been solved using a diagonalization technique in the two coordinates $r$ and $z$. The imposed parity of the functions guarantees the regularity conditions at the origin needed to solve the Helmholtz equations [35].

In our simulations we have used 32 collocation points in the vertical direction $z$, 320 Fourier modes in the azimuthal direction, and 200 points in the radial direction. A time step of $5\times10^{-4}$ has proved to be sufficient to achieve convergence. It should be noted that the spatial resolution required to accurately resolve the arising patterns is very large. This is due to the large size of the container ($\Gamma=11$) and to the sharp boundary layers of the concentration field in binary mixtures. As a result, the 3D simulations presented in this paper turn out to be extremely costly.

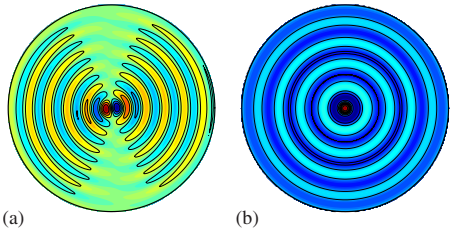


FIG. 1. (Color online) Contour plots of temperature at $z=0.5d$ during the linear transient, showing the structure of (a) an $m=1$ and (b) an $m=0$ azimuthal mode, which are the critical modes for a $\Gamma=11$ and a $\Gamma=10.5$ cylinder, respectively. The linear transient is independent of the Rayleigh number.

## III. RESULTS

In this section we present results for a water-ethanol mixture with parameters $S=-0.09$, $\sigma=24$, and $\tau=0.008$. We analyze pattern formation near the onset of convection in cylinders of aspect ratio $\Gamma=11$. This choice of parameters is motivated by the experiments of Lerman *et al.* [16–18], and are the same as those used in the linear analysis of Mercader *et al.* [21]. We tested our time-evolution code with the linear stability results, and the critical Rayleigh number $R_c=1916.2$ and frequency $\omega_c=6.157$ in our simulations agree well with the values reported in [21]. Additionally, we have considered a $\Gamma=10.5$ cell, to analyze variations in the dynamics in a slightly different aspect ratio cell.

As an indication of the patterns arising close to the convection threshold, we have explored the following ranges of values of the control parameter in the neighborhood of the critical Rayleigh number: $\varepsilon\in[-1.174\times10^{-3},9.263\times10^{-3}]$ for the $\Gamma=11$ cell, and $\varepsilon\in[8.345\times10^{-4},3.974\times10^{-3}]$ for the $\Gamma=10.5$ cell. In the following, a representative selection of the simulations is presented to explain the main features of the dynamics we have obtained. The linear transients are independent of the Rayleigh number and will be described in Sec. III A. The nonlinear evolution depends on the value of the Rayleigh number, and different behaviors are observed for subcritical or slightly supercritical values of the control parameter (Sec. III B) and for supercritical values (Sec. III C). The differences observed in the nonlinear evolution for the $\Gamma=10.5$ cell will be discussed in Sec. III D.

### A. Linear transients

We begin the simulations by using as initial condition a profile having a small Gaussian noise in the temperature field of the critical mode and zero in the remaining modes and fields, and allow the system to evolve. The linear transient for supercritical values of the Rayleigh number is similar in all the cases.

In the $\Gamma=11$ cell, $m=1$ is the selected mode at the onset of convection; its structure can be visualized in Fig. 1(a). The pattern consists of radially traveling waves and is nearly a standing wave in the azimuthal direction. This structure results from the superposition of two counterpropagating spiral modes, which correspond to the spiral eigenfunctions obtained in the linear stability analysis [21]. The eigenfunctions

TABLE I. Critical values of the Rayleigh number and frequency of the first three modes that become unstable for a $\Gamma=11$ and a $\Gamma=10.5$ cylinder. While the dominant modes are odd in the $\Gamma=11$ cylinder, they are even in the $\Gamma=10.5$ cell.

| $\Gamma=11$ | $n$ | $R$ | $\omega_c$ | $\Gamma=10.5$ | $n$ | $R$ | $\omega_c$ |
|---|---|---|---|---|---|---|---|
| | 1 | 1916.2 | 6.157 | | 0 | 1917.4 | 6.156 |
| | 3 | 1916.7 | 6.137 | | 2 | 1917.6 | 6.145 |
| | 5 | 1917.9 | 6.095 | | 4 | 1918.6 | 6.112 |

consist of right-handed and left-handed spirals traveling in the azimuthal direction in opposite directions. The vertical symmetry of these eigenfunctions allows the generation of other dominant odd modes, which become important from a very early stage of the evolution.

A slight variation in the aspect ratio cell produces a change in the critical azimuthal mode. For the $\Gamma=10.5$ cell the $m=1$ mode is no longer dominant, and the $m=0$ mode, whose structure is plotted in Fig. 1(b), is the selected mode at the onset. In this case, modes with wave number different from $m=0$ need a much longer time to be nonlinearly generated, since they cannot be generated by the $m=0$ mode and must grow out of noise, but at a certain stage of evolution even modes are excited with an amplitude larger than that of odd modes.

These observations are in agreement with the linear stability results. As can be appreciated in Table I, which shows that the critical values of the first three modes become unstable for the two cells we are considering, the critical Rayleigh numbers of low-order odd modes are smaller than those of the low-order even modes in the $\Gamma=11$ cell, while even modes are dominant in the $\Gamma=10.5$ cell. Furthermore, the presence in the nonlinear solution of several azimuthal modes of the same order for values of the control parameter extremely close to the onset of convection indicates that the critical Rayleigh numbers corresponding to different azimuthal modes lie within a very narrow range. This fact, which agrees with experimental observations [18], is confirmed by results in Table I (i.e., the difference between the critical Rayleigh numbers for the $m=1$ and 3 modes is only 0.03%) and is at the origin of the complex nonlinear dynamics observed in this system.

### B. Nonlinear evolution for slightly subcritical and supercritical Rayleigh numbers in a $\Gamma=11$ cylinder

To obtain the evolution of the patterns for subcritical or slightly supercritical Rayleigh numbers ($R=1914, 1916, 1918$), we have proceeded as in experiments [18]. Linear transients were initially allowed to evolve at a larger Rayleigh number ($R=1924, 1934$), and once the $m=1$ azimuthal mode had reached saturation, the control parameter was reduced to the subcritical value. For this narrow range of Rayleigh numbers in the immediate neighborhood of the critical value, simulations show that repeated bursts of convection amplitude take place. When the amplitude of convection is growing, sudden collapses that bring the system back to small-amplitude states are produced. After that, the amplitude of convection begins to grow again and the process repeats aperiodically.

Variations in the convection amplitude can be observed at the top of Fig. 2, where the time series of the Nusselt number for $R=1914$ ($\varepsilon=-1.174\times10^{-3}$) is plotted in units of vertical thermal diffusion time. To visualize the behavior during the bursts of amplitude, contour plots of temperature in the midplane of the cylinder at several time instants have been included at the bottom of Fig. 2. After the linear transient, the contribution of odd modes different from the critical one produces a quite pronounced azimuthal focusing along one diameter of the cell ($t=198$). However, this localized state dies away and the system returns to a state of very small amplitude focused along three diameters ($t=239$). Convection begins again, but for this particular value of the Rayleigh number, it dies away after three bursts of amplitude.

For all the subcritical values of the control parameter we have tried, we always find that, after lengthy simulations, convection eventually ceases to persist and the system de-

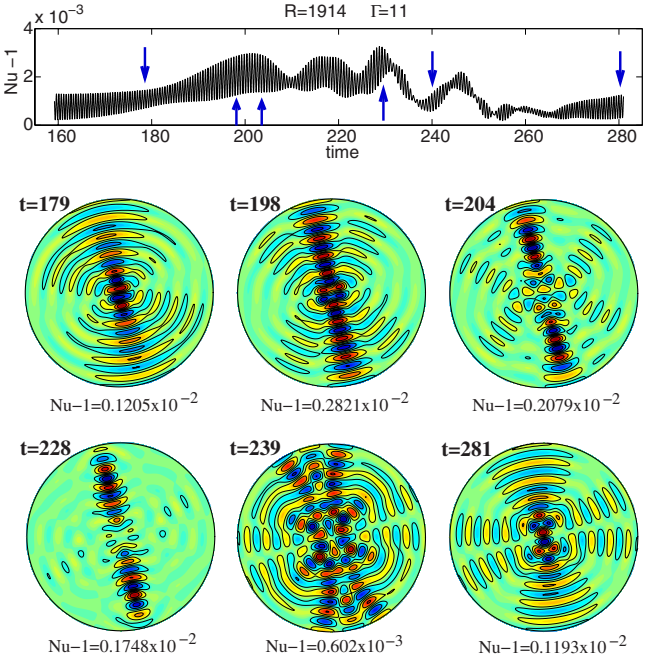


FIG. 2. (Color online) $\Gamma=11$, $R=1914$ ($\varepsilon=-1.174\times10^{-3}$). Time series (Nusselt number versus time) and contour plots of temperature at $z=0.5d$ showing the evolution of the pattern for a slightly subcritical Rayleigh number. Azimuthal focusing along one and three diameters of the cell takes place. The localized states do not persist and convection dies away.

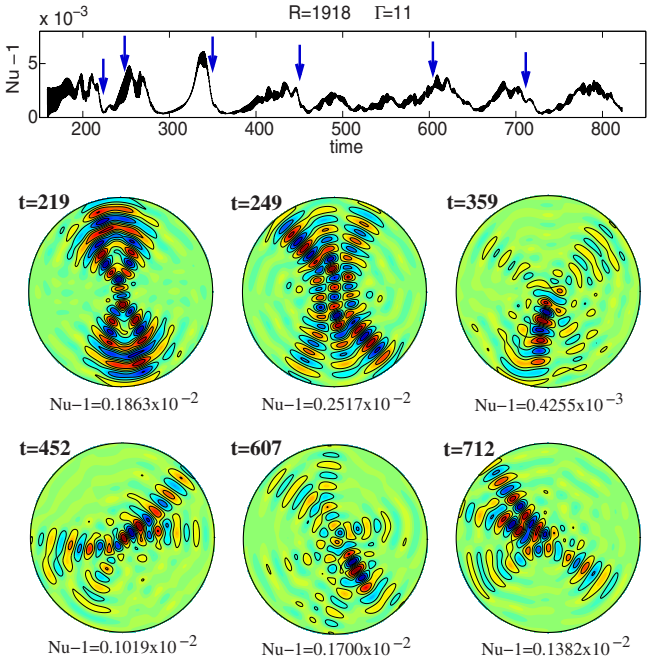


FIG. 3. (Color online) $\Gamma=11$, $R=1918$ ($\varepsilon=0.9132\times10^{-3}$). Time series (Nusselt number versus time) and contour plots of temperature at $z=0.5d$ showing the evolution of the pattern for a slightly supercritical Rayleigh number. Bursts of convection amplitude take place on the system. Convection confines radially in pulses during the collapse stages and is reestablished along bands during the burst stages.

cays to the conduction state. In contrast, for slightly supercritical values the system seems to remain indefinitely in these types of repeated transients and small amplitude states. For an example of the observed dynamics, Fig. 3 shows the Nusselt number time dependence and the complex spatial structure of the patterns at several time instants for $R=1918$ ($\varepsilon=0.9132\times10^{-3}$). The duration of the time series, shown in the picture in units of vertical thermal diffusion time, corresponds to about 28 h in real time. During the first two bursts of amplitude ($t=219,249$) convection localizes in bands. The kinetic energy bar chart showing the Fourier spectra in the azimuthal direction for the solution at $t=249$ included in Fig. 4 reveals that at this stage of the nonlinear evolution only the odd modes contribute to the solution, although modes 5 and 7 have bigger amplitudes than the critical one, as reported in the experiments [18]. As the pattern evolves, near the third burst of convection, even modes are also excited. Then, convection confines radially in pulses during the collapse stages, and is reestablished along localized bands during the bursting periods. As can be appreciated in the azimuthal Fourier spectra of the solution at $t=712$ included in Fig. 4, the even modes are nearly of the same order as the odd modes.

### C. Nonlinear evolution for supercritical Rayleigh numbers in a $\Gamma=11$ cylinder

The nonlinear evolution observed by increasing the Rayleigh number to larger supercritical values of the control parameter is different. Unlike in the near-critical case, the system does not exhibit the previous bursts and collapses in the convection amplitude. The Nusselt number increases its value progressively while blobs of disordered convection form around the cell center.

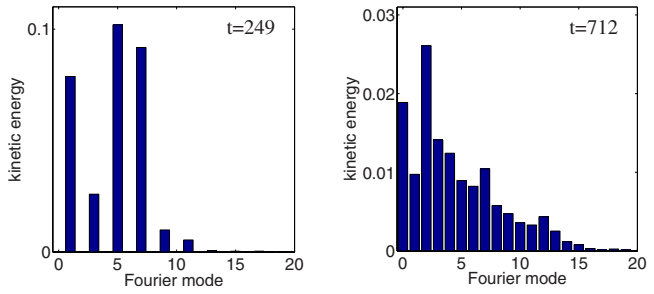


FIG. 4. (Color online) $\Gamma=11$, $R=1918$ ($\varepsilon=0.9132\times10^{-3}$). Kinetic energy bar charts showing the Fourier spectra in the azimuthal direction for the solutions at $t=249$ and 712. During the first stage of the nonlinear evolution, only the odd modes contribute to the solution. In a late stage of the evolution, even modes are also excited.

We can visualize this behavior in Fig. 5, where the temperature contour plots show the structure of the patterns at different time instants during the early stage of nonlinear evolution for $R=1934$ ($\varepsilon=9.263\times10^{-3}$). At the beginning, convection focuses again along two diameters of the cell ($t=102$), but later a localized region of squares surrounded by nearly quiescent fluid is established ($t=112$). This state does not persist either, and is replaced by a disordered blob of convection near the center of the cell ($t=119,124$).

The time series of the Nusselt number included in Fig. 6 shows the progressive increase of its value at a very slow growth rate. The contour plots at time instants ranging from $t=132$ to 731 reveal that the initially small patches of con-

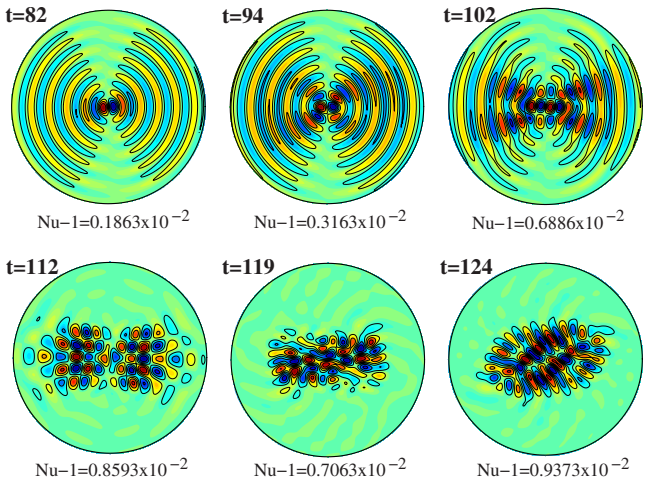


FIG. 5. (Color online) $\Gamma=11$, $R=1934$ ($\varepsilon=9.263\times10^{-3}$). Time series (Nusselt number versus time) and contour plots of temperature at $z=0.5d$ showing the evolution of the pattern during an early stage of the nonlinear transient for a supercritical Rayleigh number. A localized region of squares followed by a disordered blob of convection near the center of the cell forms.

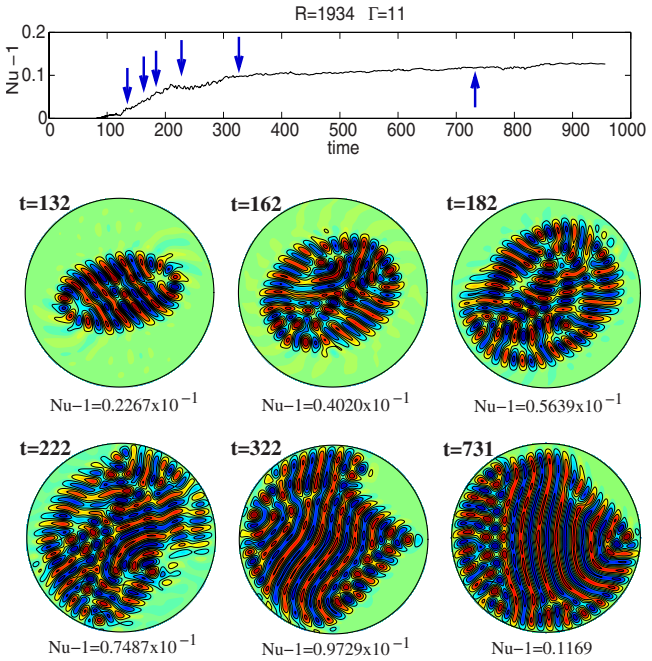


FIG. 6. (Color online) $\Gamma=11$, $R=1934$ ($\varepsilon=9.263\times10^{-3}$). Contour plots of temperature at $z=0.5d$ showing the evolution of the pattern during the late stage of the nonlinear transient for a supercritical Rayleigh number. Blobs around the center, which are surrounded by regions without convection, slowly grow and slow down until a large amplitude quasistationary state is reached.

vection, which are embedded in a region without convection, increase in size slowly. A detailed inspection of the growing phase of the blobs shows that the patterns typically consist of several competing domains of rings of traveling waves propagating essentially in the azimuthal direction, which surround an area of nearly stationary convection. When the blobs make contact with the walls, the traveling convective rolls slow down, the curved fronts that separate the convection region from that of quiescent fluid turn into abrupt straight fronts, and convection evolves filling slowly the container. Although large amplitude convection consisting of several domains of rolls with different orientations fills the whole cell at $t\approx850$, a completely stationary state has not been reached yet at the end of the simulations.

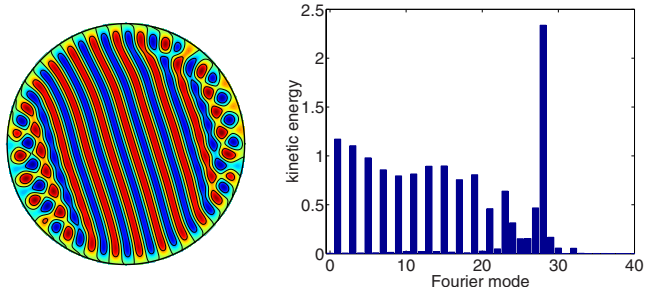


FIG. 7. (Color online) $\Gamma=11$, $R=1934$. Contour plots of temperature in $z=0.5d$ and kinetic energy bar charts showing the Fourier spectra in the azimuthal direction for the large amplitude stationary state reached for pure fluid convection ($S=0$).

The tendency of the patterns to develop quiescent areas within the domain seems to be a distinguishing feature of binary mixture convection [18], since when the separation ratio is taken to be zero (pure fluid Rayleigh-Bénard convection) in simulations starting from the state shown in Fig. 6 at $t=731$, the pattern evolves quickly toward stationary parallel stripes of convection limited by square cells filling the whole domain [36] (the final stationary state has been plotted in Fig. 7). Moreover, if the separation ratio is reestablished at its original value $S=-0.09$, simulations departing from the pure fluid stationary state show that the system rapidly shifts to a large amplitude localized state, which contains an extended region without convection. This quiescent region is slowly filled up again.

Finally, the evolution of the contribution of each azimuthal Fourier mode during the nonlinear transient can be visualized in Fig. 8, which includes the azimuthal Fourier spectrum of the solution for three different time instants. For $t=132$ odd modes are dominant, but at $t=222$ even modes are also excited. As time evolves, we can appreciate a clear shift of energy toward higher modes ($t=731$).

### D. Nonlinear evolution in a $\Gamma=10.5$ cylinder

A slight change in the aspect ratio of the cell produces variations in the dynamics. As we have mentioned when describing the linear transients in Sec. III A, the critical azimuthal mode shifts from $m=1$ to $m=0$ when the aspect ratio

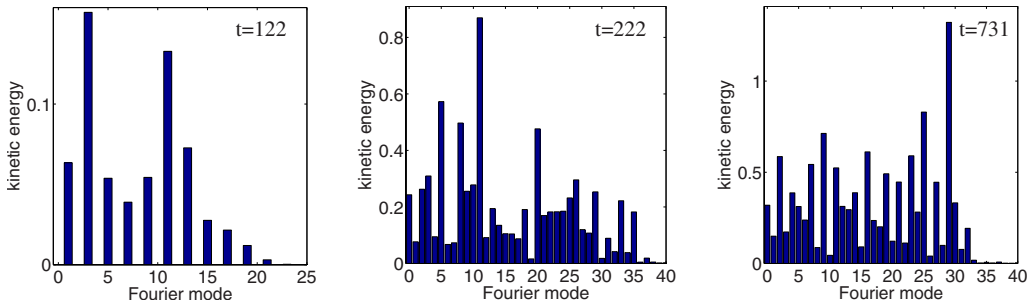


FIG. 8. (Color online) $\Gamma=11$, $R=1934$ ($\varepsilon=9.263\times10^{-3}$). Kinetic energy bar charts showing the Fourier spectra in the azimuthal direction for the solutions at $t=122$, 222, and 731. Initially, only the odd modes contribute to the solution. As the pattern evolves, even modes are also triggered and there is a displacement of energy toward higher number Fourier modes.

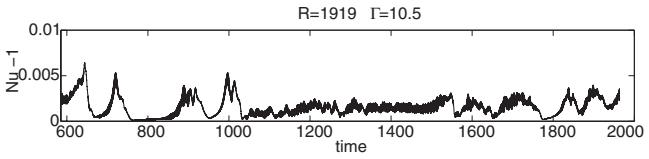


FIG. 9. $\Gamma=10.5$, $R=1919$ ($\varepsilon=8.345\times10^{-4}$). Time series (Nusselt number versus time) showing the amplitude of convection of the pattern during the nonlinear evolution for a slightly supercritical Rayleigh number. After a stage in which several bursts of convection amplitude take place, the system remains a long time in several types of localized small amplitude states. A transition to a large amplitude quasisteady pattern is not observed.

of the cylinder is reduced from $\Gamma=11$ to 10.5. Not only is the linear transient affected by the aspect ratio value, but also the nonlinear evolution for the two Rayleigh numbers we have explored, $R=1919$ ($\varepsilon=8.345\times10^{-4}$) and $R=1925$ ($\varepsilon=3.974\times10^{-3}$), presents some particular features.

The main difference in the case of the slightly supercritical value of the control parameter $R=1919$ is that the small amplitude states reached by the system do not present the regular pronounced bursts and collapses of convection amplitude exhibited in the $\Gamma=11$ cell for $R=1918$. This fact can be observed in the Nusselt number time series included in Fig. 9. In the interval $t<600$, not shown in the time series, the dynamics is essentially dominated by the $m=0$ azimuthal mode, which is the critical one. The time needed for other modes to become excited is now much larger, since the axisymmetric mode does not generate nonlinearly higher modes, so their growth is caused by the round-off errors of computations. At $t\approx600$ higher azimuthal modes begin to grow. In the range $600<t<1000$ a few growths and decays of the amplitude of convection take place, in a way similar to that described in Fig. 3, but for $t>1000$ the abrupt variations of amplitude disappear, and the system remains in several types of low amplitude localized states. These states can be confined in one or several diameters of the cell, or localized along some radius of the cell. It should be pointed out that the Nusselt time series shown in Fig. 9 is extremely long, since 1000 thermal time units correspond approximately to 35 h of real time. During the approximately 65 h of this series, the system does not evolve toward a large amplitude state, although much longer times might be required.

The nonlinear evolution for a larger value of the Rayleigh number, $R=1925$, which is summarized in Fig. 10, can be divided into four stages. During the first stage, $0<t<600$, the dynamics is dominated by the $m=0$ mode. After that, in a second stage of evolution, higher order modes are excited and the system evolves toward an extremely confined state, in which a very small convective region is surrounded by essentially quiescent fluid. This nonstationary pattern, which can be clearly visualized in the contour plot at $t=725$ of Fig. 10, bears a strong resemblance to the highly localized states observed in experiments [18]. Despite this pulsing patch of convection being long lived, at about $t=800$ the amplitude of convection begins to grow and the Nusselt number steadily increases its value. In this third stage of evolution, large amplitude convective rolls begin to fill up the cell slowly in a

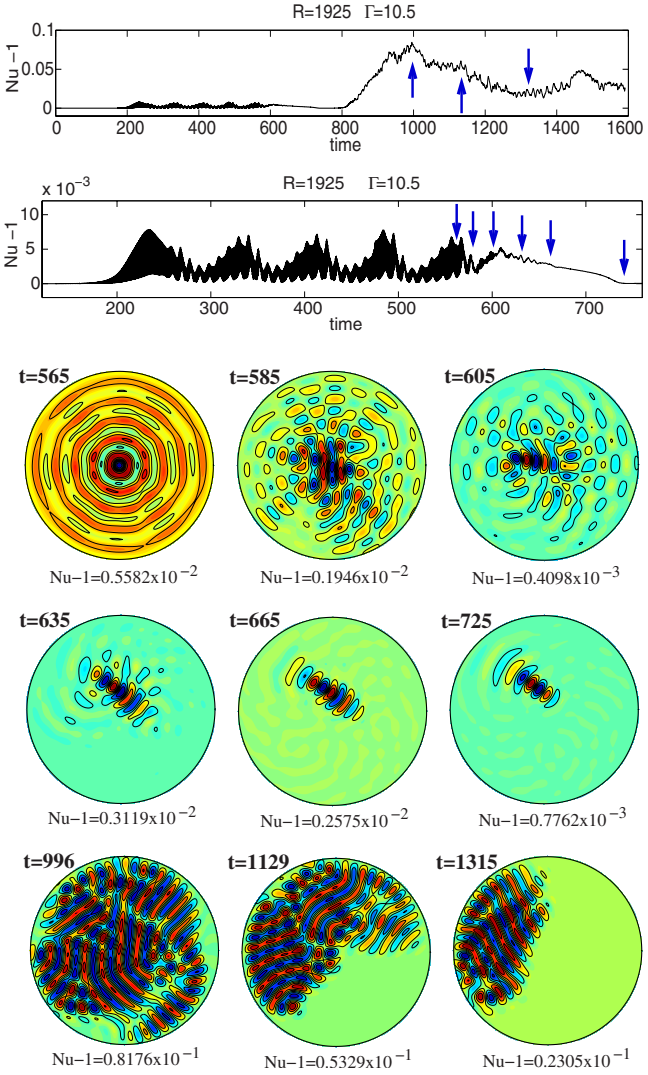


FIG. 10. (Color online) $\Gamma=10.5$, $R=1925$ ($\varepsilon=3.974\times10^{-3}$). Time series (Nusselt number versus time) and contour plots of temperature at $z=0.5d$ showing the evolution of the pattern after the early stage of the nonlinear transient for a supercritical Rayleigh number. The system remains a long time in small amplitude states, in which convection is localized in an extremely small region of the cell. However, at $t\approx800$ the amplitude of convection begins to grow steadily and convection rolls begin to fill up the cell. The patterns evolve in a similar way to that of Fig. 6, but when the cell is almost filled ($t\approx1000$), the quiescent region grows again, and the system evolves toward a confined structure.

similar way to that described in Fig. 6 for the $\Gamma=11$ cell at $R=1934$. Nevertheless, fully developed convection never fills up the cell completely, as can be appreciated in the pattern shown in Fig. 10 at $t=996$. Indeed, in a fourth stage of evolution, a steady decrease in the Nusselt number is initiated at $t\approx1000$, accounting for the fact that the quiescent regions increase their area again at a certain point of the evolution. This process of confinement can be visualized in the temperature contour plots of the pattern at $t=1129$ and 1315 included in Fig. 10. The system remains in a state of large amplitude erratic localized convection not reported in the experiments.

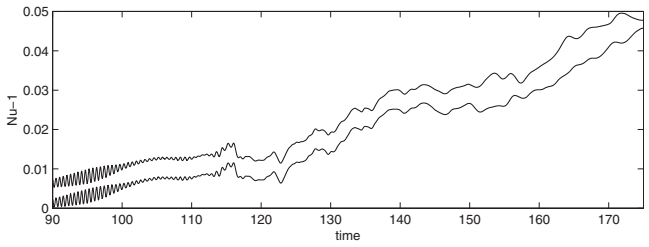


FIG. 11. Comparison of two time series of the Nusselt number obtained with different grids; the upper plot is displaced upward by 0.005 units (Upper, $200\times30\times320$; lower, $160\times30\times192$). $\Gamma=11$, $R=1934$ ($\varepsilon=9.263\times10^{-3}$).

## IV. CONCLUSIONS

In this paper we present numerical 3D simulations of convection in binary fluids with a negative separation ratio confined to a vertical cylinder in the neighborhood of the initial oscillatory instability. We consider an $S=-0.09$ water-ethanol mixture in cells of aspect ratio $\Gamma=11$ and 10.5. The choice of parameters in this paper is motivated by the experiments performed by Lerman *et al.* [16–18] on $S\approx-0.08$ mixtures in cylindrical cells of aspect ratio $\Gamma=10.91, 11.53$. To perform the simulations, we have developed a highly efficient time-evolution spectral code that solves the full convection equations in primitive variables and cylindrical coordinates. Despite this, and the increasing power of present computers, it is worth emphasizing that 3D computations on binary mixtures in moderate aspect ratio cells, such as the ones we consider, remain extremely costly.

Our confidence in the numerics is mainly based, on one hand, on tests made in other hydrodynamic and convection problems in cylindrical geometry and, on the other, on our experience using spectral codes for the simulation of binary fluid convection with small Lewis numbers in geometries different from the cylindrical one. Those systems also exhibit narrow boundary layers that can give rise to computational problems arising from lack of resolution. For instance, a poor resolution can result in collapses of amplitude. But we do not think that the collapses shown in the paper are numerical artifacts, since, with the same resolution, in some occasions convection amplitude collapses (this is the case shown in Fig. 10) while in others the system is able to remain in large amplitude states filling the cell (as in the case presented in Fig. 6).

To partially prove convergence, we have made simulations with two different grid resolutions. The two time series of the Nusselt number shown in Fig. 11 have been obtained with an intermediate grid $160\times30\times192$ and with a finer mesh $200\times30\times320$ (the last resolution has been used to obtain large amplitude states filling the whole cell and localized states). They correspond to the critical point after the linear growth in which the system decides either to go on growing in amplitude or to collapse, depending on the parameter values. As can be observed, both time series follow similar paths during the time of the integration (but not exactly the same as is typical in a chaotic system). Note that, although the Nusselt number is still growing, this is due to convection invading the cell, but the amplitude of the convecting region is completely developed, with its narrow concentration boundary layers between rolls. So we think that the two tendencies observed in the system when the states saturate after the linear growth—the tendency to collapse and the tendency to grow in amplitude and fill the cell—are well captured with the resolution we are using.

The dynamics observed within a narrow range of Rayleigh numbers around the onset of convection is of unquestionable complexity, but general agreement between the reported experimental observations and our numerical results is obtained, although some differences have also been found. The differences are probably due to non-Boussinesq effects, which can be important in experiments [17], but are not taken into account in our simulations.

The linear evolution is strongly influenced by the aspect ratio of the cell: while odd azimuthal Fourier modes dominate the dynamics in the $\Gamma=11$ cell, even modes control the early stages of evolution in the $\Gamma=10.5$ case. However, modes with wave number higher than the critical one tend to grow at much faster rates and dominate the nonlinear regime, as observed in the experiments [18]. During the nonlinear evolution, the system goes through a variety of states. Although the primary bifurcation is known to be subcritical, for subcritical values of the Rayleigh number convection dies away after some busting episodes. This absence of hysteresis in a system that undergoes a subcritical bifurcation has also been reported in experiments in rotating convection [37] and in numerical simulations of binary fluid convection in finite boxes [11]. A mechanism similar to the one described in this last reference could be responsible for the behavior reported here. For slightly supercritical Rayleigh numbers, the system can exhibit small amplitude bursting behavior for a long time (growths and collapses of convection amplitude take place), in a way that bears a strong resemblance to the dispersive chaotic states observed in large aspect ratio annular containers for small negative values of the separation ratio [5,14]. For supercritical values, on some occasions, the system evolves to form large amplitude localized states, which can combine stationary, traveling wave and quiescent regions. On other occasions, however, convection can fill the whole cell with domains of large amplitude nearly stationary rolls.

In contrast to pure fluid convection, cylindrical binary fluid convection exhibits a clear tendency to form localized and highly confined structures embedded in a background of quiescent fluid. The diversity of confined patterns is startling. On one hand, small amplitude states consisting of stripes of convection aligned along one or more cell diameters or radii are observed during the early transients for subcritical and slightly supercritical values of the control parameter. Also in this regime, when the system exhibits bursting behavior, convection can take the form of tiny highly localized pulses that are surrounded by a conductive state. On the other hand, for larger values of the Rayleigh number, localized patterns can consist of oscillatory regions of squares, disordered blobs of oscillatory convection, competing domains of traveling waves, and steady convection. States of confined convection could be persistent as suggested by our simulations for $\varepsilon=3.974\times10^{-3}$ in a $\Gamma=10.5$ cylinder, contrary to what has

been observed experimentally. Finally, for slightly greater Rayleigh numbers the system evolves slowly to a cell-filling state of convection rolls. Although the time scale of our simulations is bigger than the experimental one, we have not reached a completely stationary state.

**ACKNOWLEDGMENTS**

This work was supported by DGICYT under Grant No. FIS2006-08954 and by AGAUR under Grant No. 2005SGR-0024.

[1] D. R. Ohlsen, S. Y. Yamamoto, C. M. Surko, and P. Kolodner, Phys. Rev. Lett. **65**, 1431 (1990).
[2] P. Kolodner, J. A. Glazier, and H. Williams, Phys. Rev. Lett. **65**, 1579 (1990).
[3] P. Kolodner, Phys. Rev. A **46**, R1739 (1992).
[4] P. Kolodner, Phys. Rev. E **50**, 2731 (1994).
[5] P. Kolodner, S. Slimani, N. Aubry, and R. Lima, Physica D **85**, 165 (1995).
[6] W. Barten, M. Lücke, M. Kamps, and R. Schmitz, Phys. Rev. E **51**, 5636 (1995).
[7] W. Barten, M. Lücke, M. Kamps, and R. Schmitz, Phys. Rev. E **51**, 5662 (1995).
[8] M. Lücke, W. Barten, P. Büchel, C. Fütterer, St. Hollinger, and Ch. Jung, in *Evolution of Spontaneous Structures in Dissipative Continuous Systems*, edited by F. H. Busse and S. C. Müller (Springer-Verlag, Berlin, 1998), p. 127.
[9] D. Jung and M. Lücke, Phys. Rev. Lett. **89**, 054502 (2002).
[10] D. Jung and M. Lücke, Phys. Rev. E **72**, 026307 (2005).
[11] O. Batiste, M. Net, I. Mercader, and E. Knobloch, Phys. Rev. Lett. **86**, 2309 (2001).
[12] I. Mercader, A. Alonso, and O. Batiste, Eur. Phys. J. E **15**, 311 (2004).
[13] O. Batiste, E. Knobloch, A. Alonso, and I. Mercader, J. Fluid Mech. **560**, 149 (2006).
[14] A. Alonso, O. Batiste, A. Meseguer, and I. Mercader, Phys. Rev. E **75**, 026310 (2007).
[15] A. Alonso, O. Batiste, and I. Mercader, Eur. Phys. J. Spec. Top. **146**, 261 (2007).
[16] K. Lerman, E. Bodenschatz, D. S. Cannell, and G. Ahlers, Phys. Rev. Lett. **70**, 3572 (1993).
[17] K. Lerman, G. Ahlers, and D. S. Cannell, Phys. Rev. E **53**, R2041 (1996).
[18] K. Lerman, D. S. Cannell, and G. Ahlers, Phys. Rev. E **59**, 2975 (1999).
[19] A. La Porta and C. M. Surko, Phys. Rev. E **53**, 5916 (1996).
[20] Ch. Jung, B. Huke, and M. Lücke, Phys. Rev. Lett. **81**, 3651 (1998).
[21] I. Mercader, M. Net, and E. Knobloch, Phys. Rev. E **51**, 339 (1995).
[22] E. Millour, G. Labrosse, and E. Tric, Phys. Fluids **17**, 044102 (2005).
[23] S. Rüdiger and F. Feudel, Phys. Rev. E **62**, 4927 (2000).
[24] S. S. Leong, Numer. Heat Transf. **41**, 673 (2002).
[25] K. Borońska and L. S. Tuckerman, J. Fluid Mech. **559**, 279 (2006).
[26] J. D. Scheel, M. R. Paul, M. C. Cross, and P. F. Fischer, Phys. Rev. E **68**, 066216 (2003).
[27] J. J. Sánchez-Alvarez, E. Serre, E. Crespo del Arco, and F. H. Busse, Phys. Rev. E **72**, 036307 (2005).
[28] N. Becker, J. D. Scheel, M. C. Cross, and G. Ahlers, Phys. Rev. E **73**, 066309 (2006).
[29] F. Marqués, I. Mercader, O. Batiste, and J. López, J. Fluid Mech. **580**, 303 (2007).
[30] J. López, F. Marqués, I. Mercader, and O. Batiste, J. Fluid Mech. **590**, 187 (2007).
[31] I. Mercader, O. Batiste, and A. Alonso, J. Phys. Conf. Ser. **14**, 206 (2005).
[32] C. M. Aegerter and C. M. Surko, Phys. Rev. E **63**, 046301 (2001).
[33] G. E. Karniadakis, M. Israeli, and S. A. Orszag, J. Comput. Phys. **97**, 414 (1991).
[34] B. Fornberg, *A Practical Guide to Pseudospectral Methods* (Cambridge University Press, Cambridge, U.K., 1998).
[35] I. Mercader, M. Net, and A. Falques, Comput. Methods Appl. Mech. Eng. **91**, 1245 (1991).
[36] P. Le Gal, A. Pocheau, and V. Croquette, Phys. Rev. Lett. **54**, 2501 (1985).
[37] K. M. S. Bajaj, G. Ahlers, and W. Pesch, Phys. Rev. E **65**, 056309 (2002).